Article:
Gálvez, O, Gomez Martin, JC, Gómez, PC et al. (2 more authors) (2013) A theoretical study on the formation of iodine oxide aggregates and monohydrates. Physical Chemistry Chemical Physics, 15 (37). 15572 - 15583. ISSN 1463-9076

https://doi.org/10.1039/c3cp51219c

View Article Online
DOI: 10.1039/C3CP51219C

Theoretical study on the formation of iodine oxides aggregates and monohydrates

O. Gálvez[1*], J.C. Gómez Martín [2], P.C. Gómez[3], A. Saiz-Lopez[4] and L. F. Pacios[5]

[1] *Departamento de Física Molecular, Instituto de Estructura de la Materia, IEM-CSIC, Serrano 123, 28006 Madrid, Spain*

[2] *School of Chemistry, University of Leeds, LS2 9JT, Leeds, UK*

[3] *Departamento de Química Física I, Facultad de Química, Universidad Complutense de Madrid, 28040 Madrid, Spain*

[4] *Atmospheric Chemistry and Climate Group, Institute for Physical Chemistry Rocasolano, CSIC, Serrano 119, 28006 Madrid, Spain*

[5] *Unidad de Química y Bioquímica, Departamento de Biotecnología, E.T.S. Ingenieros de Montes, Universidad Politécnica de Madrid, 28040 Madrid, Spain*

* Correspondence to: oscar.galvez@csic.es

View Article Online
DOI: 10.1039/C3CP51219C

Abstract

Biotic and abiotic emissions of molecular iodine and iodocarbons from the sea or ice surface and the intertidal zone to the coastal/polar marine boundary layer lead to the formation of iodine oxides, which subsequently nucleate forming iodine oxide particles (IOPs). Although the link between coastal iodine emissions and ultrafine aerosol bursts is well established, the details of the nucleation mechanism have not yet been elucidated. In this paper, results of a theoretical study of a range of potentially relevant aggregation reactions of different iodine oxides, as well as complexation with water molecules, are reported. Thermochemical properties for these reactions are obtained from high level *ab initio* correlated calculations including spin-orbit corrections. The results show that the nucleation path most likely proceeds through dimerisation of I_2O_4. It is also shown that water can hinder gas-to-particle conversion to some extent, although complexation with key iodine oxides does not remove enough of these to stop IOP formation. A consistent picture of this process emerges from the theoretical study presented here and the findings of a new laboratory study reported in the accompanying paper (Gomez Martin, *et al*., 2013).

View Article Online
DOI: 10.1039/C3CP51219C

1. Introduction

The atmospheric chemistry of iodine has received considerable attention in the past two decades[1] mainly due to its potential role in ozone catalytic destruction[2, 3] and new particle formation.[4] The way in which iodine participates in atmospheric chemical processes has been the subject of a number of recent studies and is beginning to be understood.[1] It is known that intertidal seaweed beds are major producers of I_2,[4] and marine phytoplankton also liberates organoiodine species such as CH_3I. Recently, it has also been shown that the mayor global oceanic source of iodine to the marine boundary layer (MBL) is inorganic,[5, 6] and results most likely from the oxidation of iodide in the sea water surface by deposited ozone, which results in the release of HOI and I_2.[7] These iodine-bearing molecules have short photolytic lifetimes and quickly release I atoms, which are subsequently oxidized by ozone to form iodine monoxide (IO).

In coastal environments[8-10] and over Antarctic sea ice surfaces,[11] intense emission of iodine precursors (mostly I_2) results in high IO mixing ratios capable of sustaining the formation of iodine oxides that polymerize to form iodine oxide particles (IOPs). A number of laboratory studies have been conducted to investigate this process (see e.g. refs. [12-14]), although the mechanism of particle formation is not fully understood, as shown in Fig 1. Besides the uncertain photochemical properties of many iodine oxides participating in the mechanism, a major unsolved issue is the nature of the nucleating species. I_2O_4 and I_2O_5 have been identified as the most likely candidates based respectively on the observed lack of hygroscopic growth[13] and the 2:5 I:O stoichiometry of particles.[15] A gas-phase laboratory study reported indirect evidence of I_2O_3 and I_2O_4 molecules formed by recombination of IO and OIO and of OIO with itself, respectively.[16] However, I_2O_5 formation would depend on oxidation of I_2O_4 by ozone. Since oxidation of iodine oxides by ozone is highly exothermic according to our quantum calculations, this led to an alternative scheme where iodine oxides

View Article Online
DOI: 10.1039/C3CP51219C

would be sequentially oxidized by ozone, until the nucleation species I_2O_5 would be formed (see Fig. 1). Further mechanistic complexity results from the observation in aerosol flow tube studies of lower numbers of smaller IOPs at atmospheric relative humidity than formed in the absence of water vapour. This observation suggests that water molecules could form relatively stable complexes with iodine oxides such as I_2O_3 and I_2O_4, which might affect IOP formation by inhibiting their possible polymerization.[14]

The complexity and uncertainties sketched in Fig. 1 are substantiated by the lack of relevant physico-chemical parameters, such as enthalpies and Gibbs free energies of reaction, rate constants, absorption cross-sections of higher order iodine oxides (I_2O_y, y = 3-5), etc. In this context, theoretical calculations can provide valuable information complementary to laboratory results, such as the properties of potentially relevant molecular aggregates.

From a theoretical point of view, a number of previous quantum chemical studies have been carried out to explore atmospherically relevant small iodine oxides, mainly intended to elucidate their structural and thermodynamic properties (see e. g., refs.[17-25]). *Ab initio* studies in systems containing iodine atoms are difficult due to relativistic effects and to the large number of electrons which makes difficult to use large and flexible basis sets to guarantee an adequate quality of calculated geometries and frequencies in systems with several iodine atoms. Recently, a flexible basis set intended for valence-only calculations optimized for use with a shape-consistent averaged relativistic effective potential (AREP) has been developed for the iodine atom. This methodology has been employed in theoretical studies on several iodinated species,[23, 26] obtaining accurate geometries and thermodynamic properties on all the species tested.

In this work, the same methodology is used to perform *ab initio* calculations at the CCSD(T) level of theory, including spin-orbit (SO) corrections, to study the formation of aggregates of I_2O_y (y=3-5). In addition, given the prominent role attributed to water,[14, 27] the properties of

View Article Online
DOI: 10.1039/C3CP51219C

iodine oxides monohydrates $I_xO_y\cdots H_2O$ (x = 1, 2; y = 0-5) are also investigated. The *ab initio* thermochemistry reported here is used synergistically in the accompanying experimental paper,[28] in order to derive rate coefficients and dissociation rates, hence enabling new insights into the initial steps of IOP formation.

2. Methods

A shape-consistent averaged relativistic effective potential (AREP)[29] was used to replace the 46-electron core of iodine atom.[30] This formalism has been shown to account for the relativistic effects encapsulated in the core potential when used with properly optimized basis sets.[31, 32] A valence-only aug-cc-pVTZ basis set optimized for the AREP[23] following the method prescribed to construct correlated consistent basis sets for relativistic core potentials [33] was used for the iodine atom. Conventional aug-cc-pVTZ basis sets were employed for H and O atoms.

Optimized geometries and frequencies were obtained in correlated calculations at the standard second order perturbative Moller-Plesset method, MP2. Preliminary exploratory calculations for all the species were performed using the hybrid density functional theory method, B3LYP, to obtain initial geometries. For most cases, B3LYP geometric parameters (not shown) were similar to MP2 results. In order to obtain a more accurate description of thermodynamic properties, single point CCSD(T) energies were computed at the optimized MP2 geometries, and MP2 frequencies were used to obtain zero-point energy (ZPE) corrections. For some systems such as the heaviest homo- and heterodimers of the I_2O_y (y=3-5) species, due to the excessive computational cost of the calculations, B3LYP geometries and frequencies were used instead of MP2 to compute CCSD(T) energies and ZPE corrections. Note that, as mentioned above, both methodologies give very similar results. For all species, the geometries found have shown to be real minima in the potential energy surfaces, and ZPE corrections were included in the calculation of interaction energies. Spin-orbit (SO)

View Article Online
DOI: 10.1039/C3CP51219C

corrections were obtained with the pseudopotential version of the spin-orbit DFT (SODFT) method implemented in NWChem.[34] This approach uses a relativistic two-component Hamiltonian which can be applied in either a Gaussian basis set framework based on the zeroth-order regular approximation or a SO pseudopotential framework.[35] We used the latter implementation with the SO effective potential operators developed within the shape-consistent relativistic effective core potential (RECP) formalism for iodine.[29, 30] The spin-free formulation of the SODFT method is achieved by eliminating the SO operator in the Hamiltonian. For any exchange-correlation functional used in SODFT calculations, SO effects are thus discerned by comparing the spin-free result to that of the two-component approach.[35] After exploring different functionals with our RECP SO operator for iodine, the B3LYP hybrid functional was finally selected for SODFT calculations (see below). Geometries, energies, and frequencies were computed with Gaussian 09.[36] CCSD(T) energies were also obtained with MOLPRO2010.[37] SODFT-B3LYP calculations to compute SO effects were performed with NWChem.[34]

Enthalpies and free energies of formation were estimated as follows. For the lower iodine oxides, I_xO_y, being x=1,2 and y=1,2, enthalpies of formation at 0 K were calculated by subtracting theoretical atomization energies from known values of the isolated atoms (atomic Δ_fH_0 from JANAF tables[38]). The details of this procedure can be found in the report of Curtiss *et al.*[39] Then, Δ_fH_{298} and Δ_fG_{298} values were obtained by applying the following equations:

$$\Delta_fH_{298} = \Delta_fH_0 + (H_{298} - H_0)_{compound} - (H_{298} - H_0)_{elements} \quad (E1)$$

$$\Delta_fG_{298} = \Delta_fH_{298} - T(S_{compound} - S_{elements}) \quad (E2)$$

where reference data from the JANAF tables[38] for $(H_{298} - H_0)_{elements}$ and $S_{elements}$ were used. The atomic SO correction used for the iodine atom is 30.29 kJ mol^{-1}.[18] For the higher iodine oxides, I_2O_y (y=3-5), thermodynamic properties were alternatively estimated from enthalpy

View Article Online
DOI: 10.1039/C3CP51219C

changes calculated for selected reactions. To obtain the enthalpy of formation of a compound with this procedure, enthalpies of reaction have to be estimated, and knowledge of the corresponding experimental values for the other molecules involved in the reaction is required. The following reactions were selected:

$$IOIO + O_3 \rightarrow I_2O_3 + O_2 \quad \text{(R1)}$$

$$OIO + OIO \rightarrow I_2O_4 \quad \text{(R2)}$$

$$I_2O_4 + O_3 \rightarrow I_2O_5 + O_2 \quad \text{(R3)}$$

For O_3 and OIO the experimental values of Δ_fH_o 145.35 and 122 kJ mol^{-1} were employed. Due to the lack of an experimental determination of Δ_fH_o for IOIO, the high level *ab initio* calculation of Grant *et al.*[18] was used (161.5 kJ mol^{-1}). For I_2O_4 in R3, we used the estimation derived from R2. In all cases, the enthalpies of reaction for R1-R3 calculated in this work have been used to estimate the enthalpies of formation.

Topological analysis of the electron density $\rho(\mathbf{r})$ of the lowest lying structures of selected homo- and heterodimers of I_2O_y (y = 3-5) has been also carried out. $\rho(\mathbf{r})$ was obtained with from all-electron MP2/TZVPP Gaussian 09[36] calculations on optimized MP2 geometries. The critical points of $\rho(\mathbf{r})$ were located and characterized according to the Atoms in Molecules (AIM) theory[40, 41] with the program Extreme.[42] Numerical grids to render isocontour maps of $\rho(\mathbf{r})$ were computed with CheckDen[43] from the Gaussian output.

Finally, to derive rate constants and thermal dissociation lifetimes from the *ab initio* data, we have used the Master Equation Solver for Multi-Energy well Reactions (MESMER)[44, 45]. Briefly, the set of ro-vibrational energy levels in the *ab initio* potential energy surface (PES) are grouped into energy grains, and the population in each grain is described by a set of coupled differential equations that account for collisional energy transfer and dissociation within each grain. Microcanonical rate coefficients for the unimolecular reactions that occur

View Article Online
DOI: 10.1039/C3CP51219C

in each energy grain are calculated from the *ab initio* PES data. For barrierless association reactions, the Inverse Laplace Transform Method (ILT)[46, 47] can be used to calculate the microcanonical association rates from an estimate of the high pressure limiting rate coefficient for molecular association (here assumed to be equal to the corresponding collision number in each case). The microcanonical dissociation rate coefficients are then determined by detailed balance. The exponential down model is used for describing collisional energy transfer probabilities. In order to obtain an estimate of the energy transfer parameter $<\Delta E_{down}>$ for the iodine oxides, we have fitted the phenomenological rate constant and branching ratios of the IO self-reaction as a function of pressure (7-760 Torr) calculated by MESMER to the experimental data available.[16, 48] Together with the rate constant and the branching ratios of the I+OIO and IOIO product channels, $<\Delta E_{down}>$ is also treated as a floating parameter to obtain an optimal value. Such an exercise was first attempted by Gomez Martin and Plane,[49] who noted that the branching ratio of the aggregation channel was underestimated by their RRKM algorithm using $<\Delta E_{down}>\sim 300 cm^{-1}$ (for N_2). The optimal value of 500 cm^{-1} (for N_2) obtained in our exercise is somewhat higher (by about ~50%) compared to the values reported for other systems at room temperature.[50] This possibly indicates that the exponential down model does not provide an adequate description of energy transfer in this particular system. It should also be noted that the value of $<\Delta E_{down}>$ is coupled to the collision frequency between the excited adduct and the third body, which is estimated assuming a simple Lennard-Jones potential between them. An extensive investigation of this issue is however beyond the scope of the paper and we have decided to stick to the approach we adopted in this study, keeping in mind the empirical character of our choice for $<\Delta E_{down}>$. Note that in the accompanying paper the experiments are carried out in helium, and $<\Delta E_{down}>$ is chosen to be 300 cm^{-1} to account for the reduced collisional stabilization efficiency. Lennard-Jones parameters for the

View Article Online
DOI: 10.1039/C3CP51219C

interaction of the molecular complexes with air molecules are estimated following the procedure recommended by Gilbert and Smith[50] (σ ranging from 5 to 7 Å, ε = 300 K).

3. Results and Discussion

Iodine oxides

Table 1 contains thermodynamic data for iodine oxides involved in the molecular complexes studied. Total atomization energies of all the iodine oxides studied, including the electronic, ZPE and SO contributions, are available in the supporting information (SI). Our CCSD(T) results are compared with other theoretical values and experimental data when available. Enthalpies of formation obtained from MP2 or B3LYP energy calculations (not shown) were found to show large discrepancies with the experimental values. This indicates that the treatment of electron correlation at a high level of theory such as CCSD(T) is mandatory to compute reliable electronic energies.

Given that our main objective is the theoretical study of aggregates of I_2O_y (y = 3-5) and that rigorous calculations of SO effects are computationally expensive, we resorted to using the pseudopotential implementation of the SODFT method[35] as an approximation to estimate SO effects. The performance of different DFT functionals and relativistic effective potentials in SODFT calculations has been assessed elsewhere.[35, 51] The hybrid functionals ACM , PBE0, and B3LYP together with RECP SO effective potentials[29] provide reasonable estimates of bond lengths, vibrational frequencies, and dissociation energies in diatomics with Br, I, Bi, Au, and Hg atoms.[51, 52]

SODFT calculations of the SO correction on atomic iodine using ACM, PBE0, and B3LYP functionals yielded values of 2441 cm^{-1}, 2442 cm^{-1}, and 2614 cm^{-1} respectively, in good agreement with the experimental value 2534 cm^{-1}.[52] After exploring the performance of these functionals in IH, I_2 and IO molecules, we selected B3LYP to estimate SO effects. The

View Article Online
DOI: 10.1039/C3CP51219C

reliability of this selection is illustrated by comparing our B3LYP-SODFT results for the bond length, vibrational frequency, and dissociation energy of the IO molecule, 1.865 Å, 705 cm^{-1} and 2.63 eV, respectively. The corresponding results from state-of-the-art calculations by Peterson *et al.* [25] are 1.872 Å, 684 cm^{-1} and 2.39 eV, while the experimental values are 1.868 Å, 682 cm^{-1} and 2.35 ± 0.03 eV.[25] In their higher-level *ab initio* study of halogen oxides, both Grant *et al.* [18] and Peterson *et al.* [25] report for IO a contribution of molecular and atomic SO coupling of ΔE^{SO} = -14.02 kJ mol^{-1}. It is worth mentioning that using the spin-free and two-component B3LYP-SODFT energies for I and O atoms and IO molecule, our equivalent correction was estimated at -13.85 kJ mol^{-1}.

When our results for small iodine oxides at the CCSD(T) level including SO corrections are compared with the scarce experimental data available (only for IO and OIO) these are ~ 20 kJ mol^{-1} higher. In addition, our values for lower iodine oxides are also systematically larger (8 to 23 kJ mol^{-1}) than those obtained by Grant *et al.* [18] using higher quality *ab initio* methods. To evaluate our source of error, we have explored the effect of the basis set size for the test case of IO molecule. Increasing the basis size from AREP-optimized aug-cc-pVDZ to aug-cc-pVQZ, decreases $\Delta_f H_0$ from 157 to 130 kJ mol^{-1}, being this last value similar to that obtained in ref. [18] with extrapolation to the complete basis set limit. This result suggests that our error may arise mainly from the size of the basis set used (TZ), being other corrections (e.g. core-valence correction) less important. However, the size of the systems studied (the largest aggregates have 14 atoms, 4 of them iodine atoms, e.g. I_4O_{10}) and the large number of stereoisomers explored (see below) makes hardly feasible performing these calculations with the QZ basis set. Fortunately, this error is largely cancelled when quantities of interest such as enthalpies of reaction are computed. This can be checked e.g. in the dimerisation reactions of IO:

$IO + IO \rightarrow I_2O_2$ (I_2O_2 standing for IOIO, IIO_2, IOOI or OIIO) (R4)

View Article Online
DOI: 10.1039/C3CP51219C

The computed $\Delta_r H_0$ values using the heats of formation given in ref.[18] differ a maximum of only 4 kJ mol^{-1} from our calculated values using the TZ basis set. Table 1 also reveals that among the four isomers of I_2O_2, IIO_2 is predicted to be the most stable one, lying 6 kJ mol^{-1} lower in energy than IOIO, in reasonable agreement with the result of Grant *et al.* [18] Note that we have taken advantage of this error cancelation to evaluate the heats of formation of the higher iodine oxides (I_2O_y, y=3-5) using selected chemical reactions R1-R3, as described in Methods. The results obtained for I_2O_3 and I_2O_4 (Table 1) are in good agreement which those of Kaltsoyannis and Plane,[19] although a larger difference arises for the enthalpy of I_2O_5.

Geometries optimized at MP2 calculations for all the iodine species involved in the molecular complexes studied are displayed in Fig. 2. Atom coordinates of all species studied in this work are available in the SI. Bond distances show well defined patterns that provide information about the nature of bonding. For example, I-O bond lengths are about 1.75 Å in IOO moieties, about 1.80 Å in XIO (X = I, O) moieties, and about 2.0 Å in IOI moieties. The reference bond length in the diatomic IO oxide, 1.86 Å, lies between the latter values. However, I-I bond lengths in IIO (2.75 Å), IIOO (2.79 Å), and OIIO (2.88 Å) are longer than the reference value in the diatomic I_2 (2.66 Å). While these geometry parameters only represent a piece of information, it is worth noting that such variations suggest that I-O bonds in most oxides are stronger than in the isolated IO diatomic molecule and I-I bonds weaker than in I_2.

Iodine oxides monohydrates

MP2 optimized structures of the iodine oxides monohydrates studied in this work are displayed in Figs. 3-5, and their thermodynamic data (enthalpies at 298 K and standard free energies at 273 and 298 K for complex formation from its molecular constituents) are shown in Table 2. We have also included the complexes of water with atomic and molecular iodine to complete the set of possible monohydrates formed with the iodine species involved in the

View Article Online
DOI: 10.1039/C3CP51219C

IOPs formation processes sketched in Fig. 1. In the case of I_2O_2, we have only included the two most stable isomers (see the preceding subsection).

In some complexes, the lowest lying structures present an intermolecular halogen bonding (XB) interaction[53-55] instead of the conventional hydrogen bonding (HB). For the monohydrates of I_2 and IIO, only one stable structure that corresponds to the XB interaction (with similar intermolecular distances of 2.9 and 3.0 Å, respectively) was found in our MP2 optimizations (Fig. 3). For the monohydrates of I, IO, and IOI, stable structures showing both interactions were found (Fig. 3), displaying significant differences in their thermodynamic data. In fact, while the IO···H_2O complex shows virtually indistinguishable Δ_rH and Δ_rG^0 values and the I···H_2O complex shows small yet noticeable thermodynamic differences, the IOI···H_2O complex exhibits considerably different enthalpies and free energies favouring the XB structure (Table 2). In a previous *ab initio* study on monohydrates of halogen oxides ClO and BrO, we demonstrated that the XB interaction in the OX···OH_2 structures shows a similar or even larger strength than hydrogen bonding in the XO···HOH arrangements.[56] The present work confirms this feature in the IO monohydrate.

The OIO···H_2O complex presents a stable structure in which both XB and HB interactions occur, giving rise to a ring-like closed I-O···O-H···I bonding arrangement (Fig. 3). The presence of the two interactions is readily noticed in the markedly greater enthalpy and standard free energy of formation of this complex with respect to the remaining triatomic iodine oxides systems (Table 2). Higher iodine oxides monohydrates, I_2O_y (y=2-5), present multiple intermolecular bonds between I_2O_y and H_2O, displaying also closed bonding arrangements (Figs. 4 and 5) and greater stabilities (Table 2). The lowest lying structures always show a XB interaction besides HB. Moreover, in the only case in which a stable HB complex was found among these I_2O_y···H_2O systems (the third conformer of I_2O_3···H_2O in Fig. 4), its thermodynamic data reveal a significantly lower stability in terms of standard free

View Article Online
DOI: 10.1039/C3CP51219C

energies with respect to the lowest lying structure (by about 16 kJmol^{-1}), and also with respect to the intermediate complex (by about 9 kJ mol^{-1}) as shown in Table 2.

The formation of iodine oxides monohydrates is exothermic since all the structures studied show clearly negative $\Delta_r H$ values (Table 2). In general, greater stabilization energies (i.e. more negative values for $\Delta_r H$) are found for increasing number of oxygen atoms in I_xO_y monohydrates, except for the highest $I_2O_5\cdots H_2O$ complex which displays similar or even smaller negative $\Delta_r H$ values than $I_2O_4\cdots H_2O$.

A recent study on the formation and growth of aerosols from iodine species[14] considered the monohydrates $I_2O_3\cdots H_2O$ and $I_2O_4\cdots H_2O$, although only complexes with HB interaction were presented. The authors reported $\Delta_r H$ = -53 and -93 kJ mol^{-1} for the I_2O_3 and I_2O_4 monohydrates, respectively, both values considerably more negative than our results. However, taking into account the large changes observed in the thermodynamic results with the level of theory, it seems likely that the treatment of electron correlation provided by B3LYP/MidiX calculations in ref. [14] could overestimate the absolute value of $\Delta_r H$. The addition of SO corrections has a minor (or even null) effect on the computed enthalpies of reaction (results not shown), with the exception of $I\cdots H_2O$ and $IO\cdots H_2O$ monohydrates (SO induce a greater stabilization of 8 and 6 kJ mol^{-1} respectively), which exhibit a single I atom and one I···O interaction (Fig. 3). The main conclusion from our computed thermodynamic properties is that the stability of these monohydrates increases for higher iodine oxides.

Standard Gibbs free energies of reaction, $\Delta_r G^0$, in Table 2 are indicative of the spontaneity of the reaction when all the species are present at unit activity (i.e. 1bar) which is obviously not the case under atmospheric conditions. Nevertheless, Gibbs free energies of reaction could be calculated from the known $\Delta_r G^0$, according to the expression:

$$\Delta_r G_t = \Delta_r G_t^0 + RT \ln Q_r \qquad \text{(E3)}$$

View Article Online
DOI: 10.1039/C3CP51219C

where Q_r is the reaction quotient. Usually, $\Delta_r G_t$ values are hard to determine because of the uncertainties in the mixing ratios of the species involved in each process. Notwithstanding these uncertainties, a rough estimate of $\Delta_r G_t$ at 298 K can be calculated in order to evaluate the spontaneity of hydration of iodine oxides under tropospheric conditions, considering a relativity humidity (RH) of 80 % and mixing ratios of iodine oxides derived from recent modelling studies of coastal MBL nucleation.[9] The result is that RT ln Q_r takes an approximate value of 40 kJ mol^{-1} in all the cases, and therefore E3 returns positive values of $\Delta_r G_{298}$ for all the hydration reactions.

In all cases, the entropy decrease and the exothermic nature of the formation of these molecular aggregates give rise to an increase of their standard Gibbs free energy of reaction with temperature. Spontaneous formation of iodine oxides monohydrates is thus favoured with decreasing temperature. However, the CCSD(T) results show that decreasing temperature from 298 to 273 K (an atmospherically relevant temperature range) implies a decrease of $\Delta_r G$ of only 2–4 kJ mol^{-1}.

Aggregates of higher iodine oxides, I_2O_y (y=3-5)

Table 3 lists the bond energies and standard free energies of aggregation for the lowest-lying structures of dimers of higher iodine oxides (I_2O_3, I_2O_4 and I_2O_5) as well as their complexes with IO or OIO (all the structures depicted in Figs. 6 and 7). Several spatial arrangements for the formation of the different conformers were tested. In the case of the complexes with IO and OIO, all these aggregates have a stoichiometry I_3O_y (y = 4-7), with unpaired electrons, feature which usually gives rise to an enhanced reactivity. I_2O_3 and I_2O_4 form stable complexes with IO and OIO, but in the case of I_2O_5, only stable dimers with OIO (but not with IO) were found. As shown in Table 3, the formation of these complexes is an exothermic process in all the cases, especially when I_2O_4 is present. In this case, I-O intermolecular

View Article Online
DOI: 10.1039/C3CP51219C

distances shorter than 2.3 Å, and comparable to typical intramolecular I-O bonds lengths, are formed. An estimation of $RT \ln Q_r$ was also carried out for these aggregation reactions, which takes values of ca. 60 kJ mol^{-1} to be added to $\Delta_r G^0_{298}$ in E3. Consequently, although large negative $\Delta_r G^0_t$ values for $I_2O_4\cdots IO$ and $I_2O_4\cdots OIO$ are found, these aggregates would not spontaneously form under tropospheric conditions.

Only one stable structure was found for the $(I_2O_3)_2$ and $(I_2O_5)_2$ homodimers, while three stereoisomers were found for $(I_2O_4)_2$, $(I_2O_3\cdots I_2O_4)$ and $(I_2O_3\cdots I_2O_5)$ complexes and up to six structures for the $(I_2O_4\cdots I_2O_5)$ heterodimer. Due to the many bonding possibilities of these molecules, other potentially bonded stereoisomers cannot be ruled out, although it is likely that global minima have been captured. All these optimized geometries are shown in Figures S1 and S2 in the Supplementary Information while their dimerisation energies (including ZPE corrections) are collected in Table S2 (SI). The lowest-lying structures shown in Fig. 7 display in all cases a well differentiated stability. However, the remaining stereoisomers above the lowest-lying structure show small energy differences, about 10 kJ mol^{-1} in some cases.

These dimers involve the formation of closed I-O arrangements with interesting bonding features such as nearly square I-O-I-O rings in some stereoisomers, particularly $(I_2O_4)_2$, which shows by far the greatest stability (Table 3). In this homodimer, the intermonomer I2···O5 = I3···O2 distances of 2.130 Å are similar to intramonomer I2-O1 = I3-O6 distances of 2.015 Å (numbering of atoms and bond critical points, BCPs, of the electron density $\rho(\mathbf{r})$ refers to Fig. 8). The topological analysis of the electron density (Table S2 in the SI) provides also values of $\rho(\mathbf{r})$, the Laplacian of $\rho(\mathbf{r})$, and negative total energy densities at intermolecular BCPs 6 and 7 not very different from those at intramolecular BCPs 2 and 9 at paths of similar atomic arrangements. Moreover, the comparison of these topological descriptors in the intermolecular paths of $(I_2O_4)_2$ with those of reference complexes with strong hydrogen- or

View Article Online
DOI: 10.1039/C3CP51219C

halogen- bonding [57-60] reveals clear covalent features in the I···O interaction. Even the electron density (Fig. 8B) shows a spatial distribution reminiscent of covalent molecules. In fact, the contours map of $\rho(\mathbf{r})$ at the plane defined by I3, O5, and I2 atoms displays an isocontour as large as $\rho(\mathbf{r})$ = 0.08 a.u. surrounding both monomers and $\rho(\mathbf{r})$ at the intermolecular BCPs 6 and 7 is about 0.10 a.u., values much higher than those found in usual complexes.[41, 57-60]

Topological data for other I_2O_y (y = 3-5) complexes (results not shown) suggest a more conventional bonding picture. Although intermolecular BCPs still show unusual features such as relatively large values of $\rho(\mathbf{r})$ and its Laplacian as well as negative total energy densities, they point to a strong intermolecular I···O interaction rather than to a virtually covalent bond as in $(I_2O_4)_2$. The topological analysis of $\rho(\mathbf{r})$ can be summarized stating that the I-O···I-O interaction seems to be a particularly attractive intermonomer link. The fact that all these dimers have at least two of these links underlies their stability.

The formation of dimers of higher iodine oxides is an exothermic process that gives negative standard free energy values even at room temperature (see Table 3). Nevertheless, if we take into account our estimated value of $RT\ln Q_r$ of 60 kJ mol^{-1} that adds to the Δ_rG^0 values given in Table 3, a negative Δ_rG is only obtained for $(I_2O_4)_2$. As found for the monohydrates, SO corrections on the enthalpies of formation of these dimers are negligible except in the two heterodimers in which IO is present (ca. 7 kJ mol^{-1}). Saunders *et al.*[14] estimated binding enthalpies for $(I_2O_3)_2$, $(I_2O_3\cdots I_2O_4)$ and $(I_2O_4)_2$ complexes at B3LYP/MixiX quantum calculations, reporting values of -119, -171 and -208 kJ mol^{-1}, respectively. As for the case of iodine oxides monohydrates, these energies are considerably larger than those reported here. However, considering the rather different levels of theory in both types of calculations, it is likely that these large energies could result from a less appropriate treatment of electron correlation in B3LYP as compared to CCSD(T) calculations.

View Article Online
DOI: 10.1039/C3CP51219C

Nonetheless, the most significant result in Table 3 is the large values of $\Delta_r H$ and $\Delta_r G^0$ obtained for the I_2O_4 homodimer, more than twice the energies of most of the other complexes, a result which points to a particularly favoured formation of $(I_2O_4)_2$. As mentioned in the introduction, the nature of the iodine oxide species that polymerize to form aerosol particles has stimulated a lively debate, being I_2O_4 and I_2O_5 the most plausible candidates. According to our thermodynamic results, $(I_2O_4)_2$ formation is much more favoured than for other possible dimers such as $I_2O_3\cdots I_2O_4$, $I_2O_4\cdots I_2O_5$, or $(I_2O_5)_2$. Furthermore, our estimated $\Delta_r G_{298}$ values suggest that only this aggregate would form spontaneously under tropospheric conditions.

These results support the idea that I_2O_4 would be the species responsible for the polymerization and formation of iodine oxide particles. This seems to be in contradiction with the observed I_2O_5 composition of dry IOPs in previous laboratory studies.[15] It has been speculated that such stoichiometry would be the result of re-structuring in the solid phase. However, the thermally induced decomposition of I_2O_5 ($5\ I_2O_4 \rightarrow 4\ I_2O_5 + I_2$) occurs at 460 K.[61] It is worth comparing the solid state structures of I_2O_4 and I_2O_5 with the structures of the aggregates calculated in the present study. Solid I_2O_4 can be described as a 'one dimensional solid' comprising -I-O-IO_2-O chains bonded together by weak interchain interactions.[61] The link between I_2O_4 moieties within a chain does not involve the I-O-I-O ring. By contrast, the solid I_2O_5 structure has a tri-dimensional network character, where the chains of O_2I-O-IO_2 units are linked by I-O-I-O rings [62]. It is interesting to note that the most stable homodimer conformers of I_2O_4 and I_2O_5 involve such I-O-I-O links. The fact that the I_2O_4 dimer intermolecular link resembles the chain link of solid I_2O_5 rather than solid I_2O_4 may be a clue to understand the polycrystalline nature and O:I stoichiometry close to 2.5 of IOPs observed in laboratory experiments.[14, 15] One could speculate that reactive collisions could occur where, instead of aggregation, the growing clusters would strip dangling oxygen atoms from smaller

View Article Online
DOI: 10.1039/C3CP51219C

oxides colliding with them, while the vacant oxygen sites would prevent the full build up of the I_2O_5 crystalline structure.

The hypothesis that the dimerisation of I_2O_4 is the key reaction for the polymerisation of iodine oxides is in good agreement with new experimental results described in the accompanying paper.[28] In this study, time-of-flight mass spectrometry was used to investigate the process of formation of iodine oxides, following the dark reaction of I_2 and O_3 in a slow flow tube. Formation of IOPs was observed during these experiments. Besides the most intense signals corresponding to IO and OIO, a noticeable peak assigned to I_2O_4 was observed in the spectra, revealing the relevance of this molecule in the iodine particle formation process. Rate theory and kinetic modelling of the experimental data based on the calculated thermochemistry show that I_2O_4 is the most plausible candidate to initiate the nucleation process. Small peaks ascribed to I_3O_y species (mainly I_3O_6 and I_3O_7) were also observed in these experiments, but they were assigned to fragments of larger aggregates. This is in agreement with our theoretical results, which predict that the formation of these aggregates would not be favoured compared to formation of higher order aggregates (as e.g. I_4O_8).

5. Atmospheric implications

In order to make a preliminary assessment of the atmospheric relevance of the molecular association processes listed in Tables 2 and 3, we have used the MESMER ILT-based algorithm to compute rate constants and thermal dissociation rates under atmospherically relevant conditions. A general caveat to this exercise is that, due to the lack of laboratory experimental data for most of these processes, the uncertainty associated to master equation calculations is necessarily large, especially regarding dissociation lifetimes. However, they can be informative about the relative importance in the environment of the different possible

View Article Online
DOI: 10.1039/C3CP51219C

aggregation processes by linking our calculated bond energies to estimates of phenomenological kinetic parameters.

Note that the accuracy of the ILT method depends on the absence of barriers for the process under study, and that there is not absolute certainty about the absence of barriers to hydration and aggregation of I_xO_y (y=3-5). This assumption is supported by the fact that scans on the relevant potential energy surfaces of these reactions do not reveal significant barriers, that only minor electronic rearrangements occur in the monomeric units after aggregation, and in particular that no bond breaking happens. Also, the experimental observation of IOPs growth having negative activation energy of -78 kJ mol^{-1} [14] supports at least the absence of large barriers to aggregation throughout the process, with the negative activation energy possibly reflecting the dissociation energy of I_2O_4 (D_0 = 98 kJ mol^{-1}). Hence, in the absence of experimental evidence to the contrary, we assume there are no barriers for the aggregation reactions under study, and use the appropriate collisional frequencies (pre-exponential factor) as the high pressure limit rate constants in the ILT algorithm. If there was a barrier, an exponential term with the corresponding activation energy would need to be included. Our approximation consists in assuming that such an exponential factor is negligible.

The results for 1 bar and 298 K listed in Table 4 confirm that the most plausible route to IOPs involves formation of stable I_4O_8 via I_2O_4 association. Lifetimes in the order of magnitude of seconds or larger are required for a species to play a role in coastal IOP formation. Assuming a monomer mixing ratio of 10 pptv and a reaction constant of 10^{-10} cm^3 $molecules^{-1}$ s^{-1}, the lifetime of such species against aggregation would be 40 s. This has to be compared with the short photolytic lifetime of OIO [63, 64] and the short lifetime against thermal decomposition of I_2O_4 calculated in the present study (both about 2-3 seconds). Thus, OIO and I_2O_4 would be bottlenecks of IOP formation under atmospheric conditions, while I_4O_8 is sufficiently long lived to aggregate to other species before falling apart. Note that most aggregates in Table 4

View Article Online
DOI: 10.1039/C3CP51219C

are too short lived to play any role in IOP formation in the MBL. Even though I_2O_3 is the most stable oxide formed initially, it appears to be a dead end which does not form any aggregate long lived enough to facilitate nucleation even at 253 K (lifetime is still well below 1 second at this temperature). It is plausible then that this oxide adds to bigger IOPs after I_4O_8 is formed. Aggregates containing I_2O_5 could become stable at low temperatures, but the path to I_2O_5 requires ozone oxidation steps, which appear to be slow according to the accompanying experimental study.[28]

Another important aspect of this exercise is the calculated percentage of hydration of the iodine oxides, since previous laboratory work has shown that the presence of water vapour hinders IOP formation.[14] Iodine oxide monohydrates are generally not very stable (see discussion above), but the large abundance of water vapour may compensate for their rapid thermal dissociation, giving rise to a significant population of hydrated oxides in steady state. As shown in Table 4, half of the I_2O_4 would be bond to water at 298 K and 80% RH, which would slow down formation of I_4O_8 by blocking the I_2O_4 halogen bonding sites, but would not stop it. At lower temperatures the monohydrates become increasingly stable, but even at 253 K the population of non-hydrated I_2O_4 would be still significant (~35%). This is relevant in cold and dry environments with high iodine loadings such as coastal Antarctica where recent new particle observations suggest an iodine source.[11]

6. Conclusions

A study of atmospherically relevant aggregation processes of iodine oxides with themselves and with water molecules has been carried out. For this purpose, high level *ab initio* calculations employing a relativistic effective potential combined with a flexible valence-only REP-optimized basis set have been performed. Calculated thermodynamic values for simple

View Article Online
DOI: 10.1039/C3CP51219C

iodine oxides species are in reasonable agreement with those obtained by other authors and with the scarce experimental results available. Spin-orbit corrections were also accounted for. These corrections provide a systematic increase of enthalpies of formation of about 20 kJ mol^{-1} per iodine atom, which consequently results in a null impact in the evaluation of reaction energetics.

The formation of iodine oxides monohydrates is an exothermic process which shows greater stabilization energies for higher iodine oxides. Although standard $\Delta_r G^0$ present negative values for the highest I_2O_3, I_2O_4 and I_2O_5 monohydrates, when estimated atmospheric mixing ratios of these species are taken into account, it is seen that these monohydrates could not be spontaneously formed at relevant tropospheric temperatures (273-298 K). Aggregation of I_2O_3, I_2O_4 and I_2O_5 with IO or OIO generates open-shell species of composition I_3O_y (y = 4-7), but only in the case of I_2O_4, these reactions are exothermic. The most notable result is that a remarkably stable I_2O_4 dimer can be formed under atmospherically relevant conditions, being much more favoured than other possible complexes or hydrates. The estimated $\Delta_r G$ suggests that only this aggregate would spontaneously form under tropospheric conditions. These theoretical results are consistent with recent experimental studies on IOP formation (ref. [14] , and the accompanying paper ref. [28]). When the stable $(I_2O_4)_2$ complex is formed, two intermolecular I···O bonds are created in a nearly square I-O-I-O ring. The topological analysis of the electron density on these inter-molecular interactions reveals a markedly covalent character, which is not present in other aggregates. These covalent features are similar to those obtained for other intra-molecular I-O bonds present in the monomers. This singular characteristic could explain the enhanced stability of this dimer.

Acknowledgments

View Article Online
DOI: 10.1039/C3CP51219C

The authors are grateful to three anonymous reviewers for their valuable comments. The authors also thank J.M.C. Plane for his valuable comments. O. G. acknowledges financial support from Ministerio de Ciencia e Innovación, "Ramón y Cajal" program, and Project FIS2010-16455. L. F. P. acknowledges financial support from Ministry of Science, Project BIO2009-07050, and Comunidad de Madrid, Grant EIADES S-0505/AMB/0296. PCG gratefully acknowledges financial support from the Spanish Ministry of Science and Innovation, Project CTQ-2008-02578/BQU and Consolider Ingenio Program 2010 CSD2009-0038.

Supplementary Information

Components of the total atomization energies for all the species studied. B3LYP/aug-cc-pVTZ dimerisation energies with ZPE corrections for all the dimer structures of iodine oxides found in geometry optimizations. MP2 optimized geometries of structures of homo- and heterodimers of I_2O_y (y = 3-5) iodine oxides, including the atomic coordinates. Bond distances and topological descriptors of critical points of the electron density in the lowest-lying structures of $(I_2O_3)_2$, $(I_2O_4)_2$, $(I_2O_4\cdots I_2O_3)$, $(I_2O_5\cdots I_2O_3)$, and $(I_2O_5\cdots I_2O_4)$ dimers.

Table 1. Enthalpies of formation at 0 and 298 K, absolute entropies at 298 K, and standard free energies of formation at 298 K of iodine oxides.

Species	$\Delta_f H_0$			$\Delta_f H_{298}$			S_{298}		$\Delta_f G^0_{298}$	
	CCSD(T)	Calc	Exp	CCSD(T)	Calc	Exp	MP2	Exp	CCSD(T)	Exp
IO ($^2\Pi$)	139	130	122 ± 2[a]	137	128	120 ± 2[a]	240	240 ±1	114	97[a]
OIO ($^2B_1$)	144	123	122 ± 2[b]	140	120	118 ± 2[b]	279	281 ± 4	135	113[b]
IOI ($^1A_1$)	122	114	124 ± 25 (est)	117	108	120 ± 25 (est)	305	308 ± 4	91	93 (est)
IIO ($^1A'$)	181	164	110 ± 40 (est)	176	158	107 ± 40 (est)	316	330 ± 4	147	73 (est)
IIO_2 ($^1A'$)	171	148		165	138		338		160	
IOIO (^1A)	177	162		172	152		347		164	
IOOI (^1A)	201	186		195	178		334		191	
OIIO (^1A)	285	263		281	259		84		272	
I_2O_3 ($^1A'$)	80	78		73	64		88		90	
I_2O_4 (^1A)	144	131		136	111		96		183	
I_2O_5 (^1A)	75	54		66	33		100		144	

$\Delta_f H$ and $\Delta_f G$ in kJ mol^{-1}, S_{298} in J K^{-1} mol^{-1}. CCSD(T) data, including SO corrections, (with geometries obtained at MP2 level) are calculated following Curtiss *et al.*[39] procedure (see text). Absolute entropies correspond to calculations of frequencies at the MP2 level. Theoretical values ("Calc") are taken from ref.[18] for I_xO_y (y=1,2) and ref. [19] for y>2. Experimental values ("Exp") are from [a] Dooley *et al.*[65] and [b] Gomez Martin and Plane.[49] "est" means estimated and has been obtained from JANAF tables.[38]

View Article Online
DOI: 10.1039/C3CP51219C

Table 2. Enthalpies of reaction (or bond energies) and standard free energies of reaction for the hydration of atomic and molecular iodine and relevant iodine oxides (values in kJ mol^{-1}).

Complex	Interaction [a]	$\Delta_r H_{298}$ [b]	$\Delta_r G^0_{298}$	$\Delta_r G^0_{273}$
$I\cdots H_2O$	XB	-20	6	4
	HB	-6	10	9
$I_2\cdots H_2O$	XB	-14	11	9
$IO\cdots H_2O$	XB	-12	8	6
	HB	-16	8	6
$OIO\cdots H_2O$	XHB	-27	0	-2
$IOI\cdots H_2O$	XB	-21	7	4
	HB	-12	12	10
$IIO\cdots H_2O$	XB	-9	15	12
$IIO_2\cdots H_2O$	XHB	-32	2	-1
	XB	-9	12	10
$IOIO\cdots H_2O$	XHB-1	-30	6	3
	XHB-2	-20	15	12
$I_2O_3\cdots H_2O$	XHB-1	-36	1	-3
	XHB-2	-29	6	3
	HB	-20	14	11
$I_2O_4\cdots H_2O$	XHB-1	-53	-11	-14
	XHB-2	-43	-2	-6
	XHB-3	-36	-1	-4
	XHB-4	-31	5	2
$I_2O_5\cdots H_2O$	XHB-1	-50	-7	-11
	XHB-2	-41	-4	-7
	XHB-3	-36	1	-2

[a] XB means halogen bonding, HB means hydrogen bonding, and XHB indicates the occurrence of both interactions in the complex. [b] $\Delta_r H$ and $\Delta_r G^0_t$ from CCSD(T)//MP2/aug-cc-pVTZ calculations.

View Article Online
DOI: 10.1039/C3CP51219C

Table 3. Enthalpies of reaction (or bond energies) and standard free energies of reaction for the aggregation of relevant iodine oxides (values in kJ mol^{-1}).

Dimer	$\Delta_r H_0$ [a]	$\Delta_r H_{298}$	$\Delta_r G^0_{273}$	$\Delta_r G^0_{298}$
$I_2O_3\cdots IO$	-8	-14	17	20
$I_2O_3\cdots OIO$	-15	-16	21	24
$I_2O_4\cdots IO$	-55	-63	-19	-15
$I_2O_4\cdots OIO$	-72	-74	-27	-22
$I_2O_5\cdots OIO$	-31	-33	20	25
$I_2O_3\cdots I_2O_3$	-59	-56	-15	-11
$I_2O_4\cdots I_2O_4$	-142	-141	-88	-83
$I_2O_5\cdots I_2O_5$ [b]	-88	-87	-37	-32
$I_2O_3\cdots I_2O_4$ [b]	-80	-78	-29	-25
$I_2O_3\cdots I_2O_5$	-86	-83	-35	-30
$I_2O_4\cdots I_2O_5$ [b]	-107	-106	-53	-48

[a] Calculations at CCSD(T)//MP2/aug-cc-pVTZ level of theory. [b] Optimized geometries and ZPE corrections calculated at B3LYP level.

View Article Online
DOI: 10.1039/C3CP51219C

Table 4. Association rate coefficients and lifetimes against thermal decomposition for iodine oxides, adducts and monohydrates at 1 bar and 298 K from Master Equation calculations.

Association	k / 10^{-10} cm^3 molecule^{-1} s^{-1}	**lifetime /s**	**hydration %** [a]
IO + IO → IOIO	1.16	583	
IO + OIO → I_2O_3	1.30	1.67×10^{11}	
OIO + OIO → I_2O_4	0.670	2.3	
I_2O_4 + IO → I_2O_4···IO	0.575	4.14×10^{-6}	
I_2O_4 + OIO → I_2O_4···OIO	0.140	5.66×10^{-6}	
I_2O_5 + OIO → I_2O_5···OIO	8.9×10^{-3}	2.97×10^{-9}	
I_2O_3 + I_2O_3 → I_2O_3···I_2O_3	0.22	1.11×10^{-7}	
I_2O_3 + I_2O_4 → I_2O_3···I_2O_4	0.84	2.08×10^{-5}	
I_2O_3 + I_2O_5 → I_2O_3···I_2O_5	1.85	1.81×10^{-4}	
I_2O_4 + I_2O_4 → I_2O_4···I_2O_4	2.90	1.25×10^{5}	
I_2O_4 + I_2O_5 → I_2O_4···I_2O_5	2.30	7.46×10^{-2}	
I_2O_5 + I_2O_5 → I_2O_5···I_2O_5	1.92	2.94×10^{-4}	
IO + H_2O → IO···H_2O	7.0×10^{-4}	5.00×10^{-9}	< 1
OIO + H_2O → OIO···H_2O	5.3×10^{-3}	1.85×10^{-8}	< 1
IOIO + H_2O → IOIO···H_2O	1.4×10^{-3}	1.37×10^{-8}	< 1
I_2O_3 + H_2O → I_2O_3···H_2O	7.4×10^{-3}	2.99×10^{-8}	< 1
I_2O_4 + H_2O → I_2O_4···H_2O	2.9×10^{-2}	5.38×10^{-7}	49
I_2O_5 + H_2O → I_2O_5···H_2O	2.5×10^{-2}	1.61×10^{-7}	20

[a] Steady state percentage of iodine oxide concentration hydrated for 80% RH and 298 K

View Article Online
DOI: 10.1039/C3CP51219C

Figure captions

Figure 1. Scheme of iodine chemistry of the IOPs formation in the atmosphere.

Figure 2. MP2 optimized geometries of iodine species involved in the molecular complexes studied. Bond distances in Angstrom.

Figure 3. MP2 optimized geometries of lower iodine oxides monohydrates. XB indicates a halogen bonding interaction, HB indicates hydrogen bonding, and XHB indicates the occurrence of both interactions. Intermolecular bond distances in Angstrom.

Figure 4. Same as for Fig. 3 for monohydrates of I_2O_2 and I_2O_3.

Figure 5. Same as for Fig. 3 for monohydrates of I_2O_4 and I_2O_5.

Figure 6. MP2 optimized geometries of the lowest-lying structures of iodine oxides aggregates of I_3O_y (y = 4-7) composition. Bond distances in Angstrom. I-O bonds are arbitrarily drawn as sticks or dashed lines depending on whether the interatomic distances are shorter or longer than 2.4 Å, respectively.

Figure 7. Optimized geometries of the lowest-lying structures of homo- and heterodimers of I_2O_y (y=3-5) iodine oxides at MP2 level, with the exception of $(I_2O_5)_2$ and $I_2O_4\cdots I_2O_5$ in which B3LYP method was used instead. Bond distances in Angstrom. I-O bonds are arbitrarily drawn as sticks or dashed lines depending on whether the interatomic distances are shorter or longer than 2.4 Å, respectively.

Figure 8. **A.** Two views of the MP2 optimized geometry of the lowest-lying structure of I_2O_4 dimer depicted as sticks diagrams with I and O atoms coloured violet and red, respectively. The green sphere indicates the ring critical point and blue spheres indicate bond critical points of the electron density $\rho(\mathbf{r})$. **B.** Isocontours map of $\rho(\mathbf{r})$ at the plane defined by I3, O5, and I2 atoms in the labelled geometry drawn above. The outermost contour is $\rho(\mathbf{r})$ = 0.001 a.u. and the remaining contours are 2×10^n, 4×10^n, and 8×10^n a.u., with n = –3, –2, –1, 0, +1, and +2.

View Article Online
DOI: 10.1039/C3CP51219C

References

1. A. Saiz-Lopez, J. M. C. Plane, A. Baker, L. Carpenter, R. von Glasow, J. C. Gómez Martín, G. McFiggans and R. Saunders, *Chem. Rev.*, 2012, **112**, 1773–1804.
2. K. A. Read, A. S. Mahajan, L. J. Carpenter, M. J. Evans, B. V. E. Faria, D. E. Heard, J. R. Hopkins, J. D. Lee, S. J. Moller, A. C. Lewis, L. Mendes, J. B. McQuaid, H. Oetjen, A. Saiz-Lopez, M. J. Pilling and J. M. C. Plane, *Nature*, 2008, **453**, 1232-1235.
3. A. Saiz-Lopez, A. S. Mahajan, R. A. Salmon, S. J.-B. Bauguitte, A. E. Jones, H. K. Roscoe and J. M. C. Plane, *Science*, 2007, **317**, 348-351.
4. C. D. O'Dowd, J. L. Jimenez, R. Bahreini, R. C. Flagan, J. H. Seinfeld, K. Hameri, L. Pirjola, M. Kulmala, S. G. Jennings and T. Hoffmann, *Nature*, 2002, **417**, 632-636.
5. C. E. Jones, K. E. Hornsby, R. Sommariva, R. M. Dunk, R. von Glasow, G. McFiggans and L. J. Carpenter, *Geophys. Res. Lett.*, 2010, **37**, L18804.
6. A. S. Mahajan, J. M. C. Plane, H. Oetjen, L. Mendes, R. W. Saunders, A. Saiz-Lopez, C. E. Jones, L. J. Carpenter and G. B. McFiggans, *Atmos. Chem. Phys.*, 2010, **10**, 4611-4624.
7. L. J. Carpenter, S. M. MacDonald, M. D. Shaw, R. Kumar, R. W. Saunders, R. Parthipan, J. Wilson and J. M. C. Plane, *Nature Geosci*, 2013, **6**, 108-111.
8. A. S. Mahajan, H. Oetjen, A. Saiz-Lopez, J. D. Lee, G. B. McFiggans and J. M. C. Plane, *Geophys. Res. Lett.*, 2009, **36**, L16803, doi:16810.11029/12009GL038018.
9. A. S. Mahajan, M. Sorribas, J. C. Gómez Martín, S. M. MacDonald, M. Gil, J. M. C. Plane and A. Saiz-Lopez, *Atmos. Chem. Phys.*, 2010, **10**, 27227-27253.
10. A. Saiz-Lopez and J. M. C. Plane, *Geophys. Res. Lett.*, 2004, **31**, L04112.
11. H. M. Atkinson, R.-J. Huang, R. Chance, H. K. Roscoe, C. Hughes, B. Davison, A. Schönhardt, A. S. Mahajan, A. Saiz-Lopez, T. Hoffmann and P. S. Liss, *Atmos. Chem. Phys.*, 2012, **12**, 11229-11244.
12. J. B. Burkholder, J. Curtius, A. R. Ravishankara and E. R. Lovejoy, *Atmos. Chem. Phys.*, 2004, **4**, 19-34.
13. J. L. Jimenez, R. Bahreini, D. R. Cocker, III, H. Zhuang, V. Varutbangkul, R. C. Flagan, J. H. Seinfeld, C. D. O'Dowd and T. Hoffmann, *J. Geophys. Res.*, 2003, **108**, 4318.
14. R. W. Saunders, A. S. Mahajan, J. C. Gómez Martín, R. Kumar and J. M. C. Plane, *Z. Phys. Chem.*, 2010, **224**, 1095-1117.
15. R. W. Saunders and J. M. C. Plane, *Environ. Chem.*, 2005, **2**, 299-303.
16. J. C. Gómez Martín, P. Spietz and J. P. Burrows, *J. Phys. Chem. A*, 2007, **111**, 306-320.
17. R. J. Berry, J. Yuan, A. Misra and P. Marshall, *J. Phys. Chem. A*, 1998, **102**, 5182-5188.
18. D. J. Grant, E. B. Garner, M. H. Matus, M. T. Nguyen, K. A. Peterson, J. S. Francisco and D. A. Dixon, *J. Phys. Chem. A*, 2010, **114**, 4254-4265.
19. N. Kaltsoyannis and J. M. C. Plane, *PCCP*, 2008, **10**, 1723-1733.
20. P. Marshall, in *Adv. Quantum Chem.*, ed. E. G. a. M. S. J. Michael, Academic Press, London2008, vol. Volume 55, pp. 159-175.
21. V. S. Melissas, D. K. Papayannis and A. M. Kosmas, *J. Mol. Struct.-Theochem*, 2003, **626**, 263-269.
22. A. Misra and P. Marshall, *J. Phys. Chem. A*, 1998, **102**, 9056-9060.
23. L. F. Pacios and O. J. Gálvez, *J. Chem. Theory Comput.*, 2010, **6**, 1738-1752.
24. K. A. Peterson, *Mol. Phys.*, 2010, **108**, 393- 408
25. K. A. Peterson, B. C. Shepler, D. Figgen and H. Stoll, *J. Phys. Chem. A*, 2006, **110**, 13877-13883.
26. L. F. Pacios, P. C. Gómez and O. Gálvez, *J. Phys. Chem. A*, 2011, **115**, 12616-12623.
27. B. J. Murray, A. E. Haddrell, S. Peppe, J. F. Davies, J. P. Reid, D. O'Sullivan, H. C. Price, R. Kumar, R. W. Saunders, J. M. C. Plane, N. S. Umo and T. W. Wilson, *Atmos. Chem. Phys.*, 2012, **12**, 8575-8587.
28. J. C. Gómez Martin, O. Gálvez, M. T. Baeza-Romero, T. Ingham, J. M. C. Plane and M. A. Blitz, *Submitted*, 2013.
29. L. F. Pacios and P. A. Christiansen, *J. Chem. Phys.*, 1985, **82**, 2664-2671.
30. L. A. LaJohn, P. A. Christiansen, R. B. Ross, T. Atashroo and W. C. Ermler, *J. Chem. Phys.*, 1987, **87**, 2812-2824.

View Article Online
DOI: 10.1039/C3CP51219C

31. P. A. Christiansen, *J. Chem. Phys.*, 2000, **112**, 10070-10074.
32. W. C. Ermler, R. B. Ross and P. A. Christiansen, *Adv. Quantum Chem.*, 1988, **19**, 139-182.
33. J. M. L. Martin and A. Sundermann, *J. Chem. Phys.*, 2001, **114**, 3408-3420.
34. M. Valiev, E. J. Bylaska, N. Govind, K. Kowalski, T. P. Straatsma, H. J. J. Van Dam, D. Wang, J. Nieplocha, E. Apra, T. L. Windus and W. A. de Jong, *Comput. Phys. Commun.*, 2010, **181**, 1477-1489.
35. P. Nichols, N. Govind, E. J. Bylaska and W. A. de Jong, *J. Chem. Theory Comput.*, 2009, **5**, 491-499.
36. M. J. Frisch, G. W. Trucks, H. B. Schlegel, G. E. Scuseria, M. A. Robb, J. R. Cheeseman, G. Scalmani, V. Barone, B. Mennucci, G. A. Petersson, H. Nakatsuji, M. Caricato, X. Li, H. P. Hratchian, A. F. Izmaylov, J. Bloino, G. Zheng, J. L. Sonnenberg, M. Hada, M. Ehara, K. Toyota, R. Fukuda, J. Hasegawa, M. Ishida, T. Nakajima, Y. Honda, O. Kitao, H. Nakai, T. Vreven, J. J. A. Montgomery, J. E. Peralta, F. Ogliaro, M. Bearpark, J. J. Heyd, E. Brothers, K. N. Kudin, V. N. Staroverov, R. Kobayashi, J. Normand, K. Raghavachari, A. Rendell, J. C. Burant, S. S. Iyengar, J. Tomasi, M. Cossi, N. Rega, J. M. Millam, M. Klene, J. E. Knox, J. B. Cross, V. Bakken, C. Adamo, J. Jaramillo, R. Gomperts, R. E. Stratmann, O. Yazyev, A. J. Austin, R. Cammi, C. Pomelli, J. W. Ochterski, R. L. Martin, K. Morokuma, V. G. Zakrzewski, G. A. Voth, P. Salvador, J. J. Dannenberg, S. Dapprich, A. D. Daniels, O. Farkas, J. B. Foresman, J. V. Ortiz, J. Cioslowski and D. J. Fox, *Gaussian 09, Revision A.02*, Wallingford CT, 2009.
37. H.-J. Werner, P. J. Knowles, G. Knizia, F. R. Manby, M. Schutz, P. Celani, T. Korona, R. Lindh, A. Mitrushenkov, G. Rauhut, K. R. Shamasundar, T. B. Adler, R. D. Amos, A. Bernhardsson, A. Berning, D. L. Cooper, M. J. O. Deegan, A. J. Dobbyn, F. Eckert, E. Goll, C. Hampel, A. Hesselmann, G. Hetzer, T. Hrenar, G. Jansen, C. Koppl, Y. Liu, A. W. Lloyd, R. A. Mata, A. J. May, S. J. McNicholas, W. Meyer, M. E. Mura, A. Nicklass, D. P. O'Neill, P. Palmieri, K. Pfluger, R. Pitzer, M. Reiher, T. Shiozaki, H. Stoll, A. J. Stone, R. Tarroni, T. Thorsteinsson, M. Wang and A. Wolf, *MOLPRO, version 2010.1, a package of ab initio programs*, http://www.molpro.net, Cardiff, UK, 2012.
38. M. W. Chase, Jr., *J. Phys. Chem. Ref. Data*, 1998, **9**, 1-1951.
39. L. A. Curtiss, K. Raghavachari, P. C. Redfern and J. A. Pople, *J. Chem. Phys.*, 1997, **106**, 1063-1079.
40. R. F. W. Bader, *Atoms in Molecules: A Quantum Theory*, Clarendon, Oxford, UK, 1990.
41. P. Popelier, *Atoms in Molecules: An Introduction* Prentice-Hall, Harlow, UK, 2000.
42. F. W. Biegler-Konig, R. F. W. Bader and T. H. Hang, *J. Comput. Chem.*, 1982, **3**, 317-325.
43. L. F. Pacios and A. Fernandez, *J. Mol. Graphics Modell.*, 2009, **28**, 102-112.
44. S. H. Robertson, D. R. Glowacki, C.-H. Liang, C. Morley, R. Shannon, M. Blitz and M. J. Pilling, MESMER (Master Equation Solver for Multi-Energy Well Reactions), http://sourceforge.net/projects/mesmer.
45. D. R. Glowacki, C.-H. Liang, C. Morley, M. J. Pilling and S. H. Robertson, *J. Phys. Chem. A*, 2012, **116**, 9545-9560.
46. J. W. Davies, N. J. B. Green and M. J. Pilling, *Chem. Phys. Lett.*, 1986, **126**, 373-379.
47. S. H. Robertson, M. J. Pilling, D. L. Baulch and N. J. B. Green, *J. Phys. Chem.*, 1995, **99**, 13452-13460.
48. W. J. Bloss, D. M. Rowley, R. A. Cox and R. L. Jones, *J. Phys. Chem. A*, 2001, **105**, 7840-7854.
49. J. C. Gómez Martín and J. M. C. Plane, *Chem. Phys. Lett.*, 2009, **474**, 79-83.
50. R. G. Gilbert and S. C. Smith, *Theory of Unimolecular and Recombination Reactions*, Blackwell, Oxford, 1990.
51. J. Kim, H. Ihee and Y. S. Lee, *J. Chem. Phys.*, 2010, **133**, 144309.
52. C. E. Moore, *Atomic energy levels as derived from the analysis of optical spectra*, U.S. National Bureau of Standards, Washington, 1949.
53. P. Metrangolo, G. Resnati, T. Pilati and S. Biella, in *Halogen Bonding Fundamentals and Applications*, eds. P. Metrangolo and G. Resnati, Springer, Berlin2008, pp. 105–136.
54. P. Metrangolo, F. Meyer, T. Pilati, G. Resnati and G. Terraneo, *Angew. Chem. Int. Ed.*, 2008, **47**, 6114-6127.

View Article Online
DOI: 10.1039/C3CP51219C

55. E. Parisini, P. Metrangolo, T. Pilati, G. Resnati and G. Terraneo, *Chem. Soc. Rev.*, 2011, **40**, 2267-2278.
56. O. Gálvez, P. C. Gómez and L. F. Pacios, *J. Comput. Chem.*, 2009, **30**, 2538-2549.
57. W. D. Arnold and E. Oldfield, *J. Am. Chem. Soc.*, 2000, **122**, 12835-12841.
58. L. F. Pacios, *J. Phys. Chem. A*, 2004, **108**, 1177-1188.
59. L. F. Pacios and P. C. Gómez, *J. Phys. Chem. A*, 2004, **108**, 11783-11792.
60. L. F. Pacios, O. Galvez and P. C. Gomez, *J. Chem. Phys.*, 2005, **122**, 214307-214311.
61. H. Fjellvag and A. Kjekshus, *Acta Chem. Scand.*, 1994, **48**, 815-822.
62. K. Selte and A. Kjekshus, *Acta Chem. Scand.*, 1970, **24**, 1912.
63. J. C. Gómez Martín, S. H. Ashworth, A. S. Mahajan and J. M. C. Plane, *Geophys. Res. Lett.*, 2009, **36**, L09802, doi:09810.01029/02009GL037642.
64. J. C. Gómez Martín, P. Spietz and J. P. Burrows, *Journal of Photochemistry and Photobiology A*, 2005, **176**, 15-38.
65. K. S. Dooley, J. N. Geidosch and S. W. North, *Chem. Phys. Lett.*, 2008, **457**, 303-306.

View Article Online
DOI: 10.1039/C3CP51219C

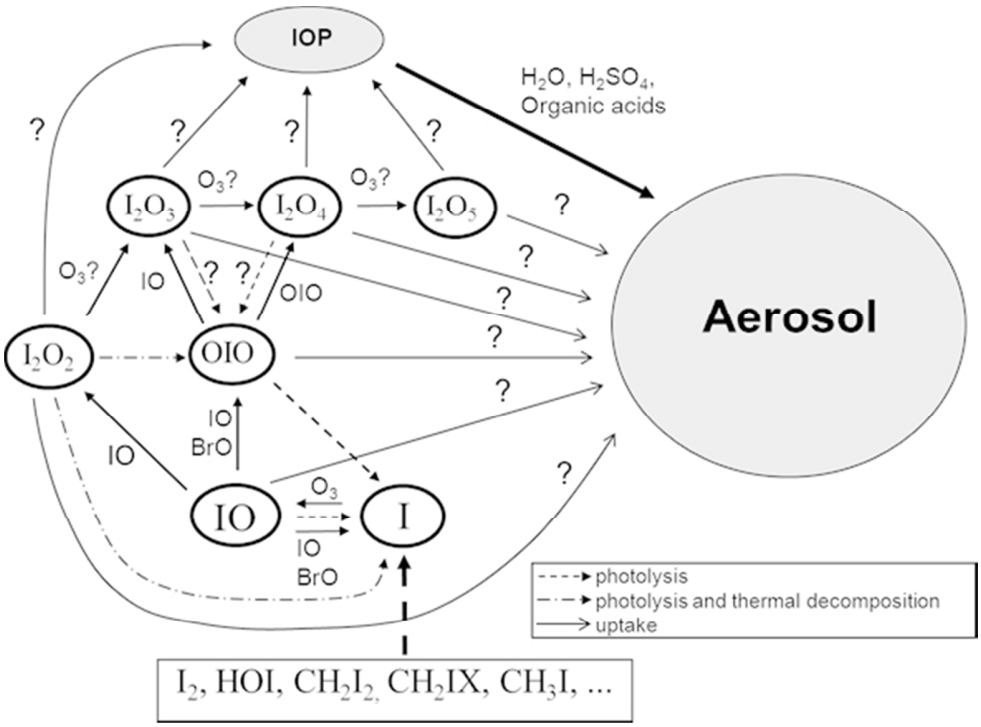

Figure 1. Caption: See manuscript
221x163mm (72 x 72 DPI)

View Article Online
DOI: 10.1039/C3CP51219C

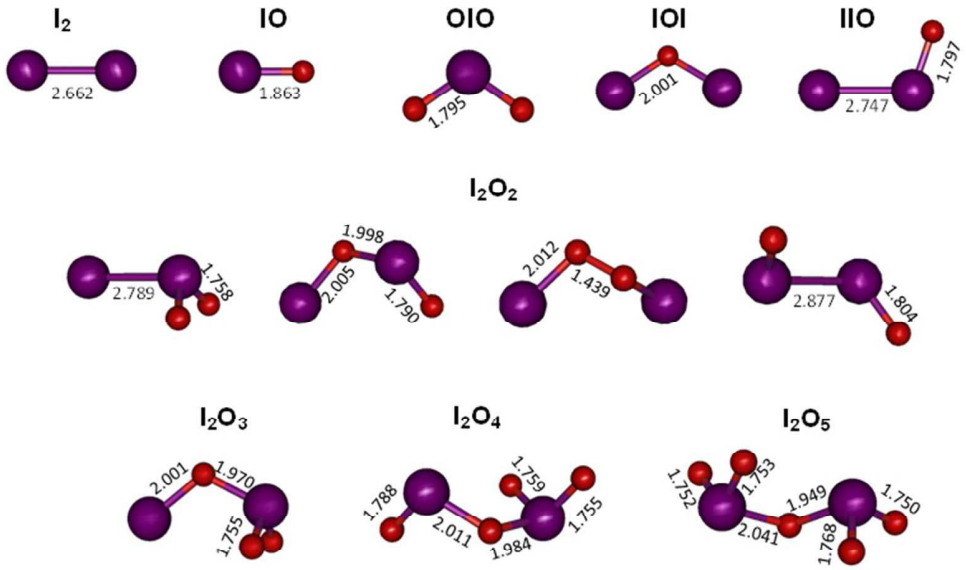

Figure 2. Caption: See manuscript
269x161mm (72 x 72 DPI)

View Article Online
DOI: 10.1039/C3CP51219C

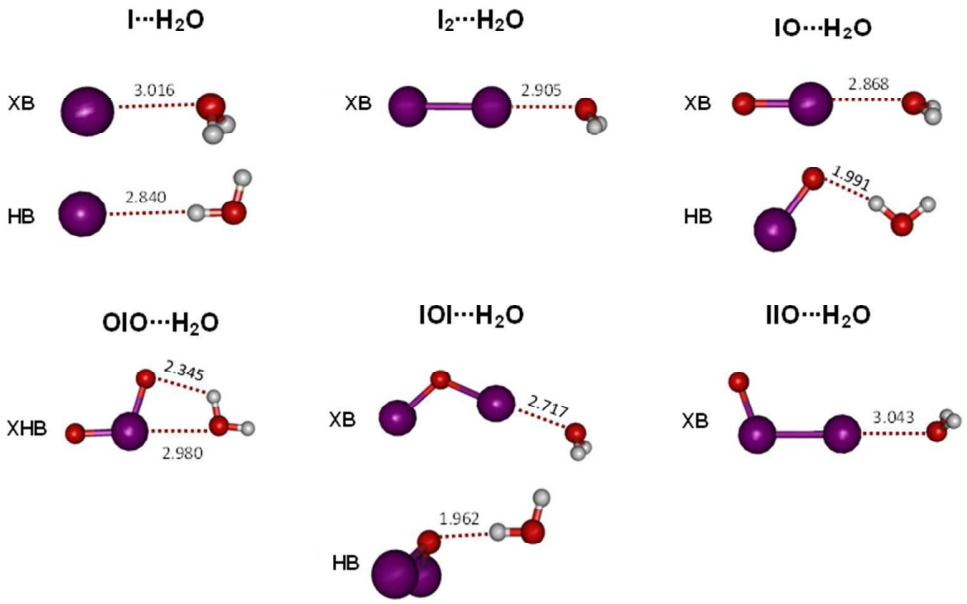

Figure 3. Caption: See manuscript
280x176mm (72 x 72 DPI)

View Article Online
DOI: 10.1039/C3CP51219C

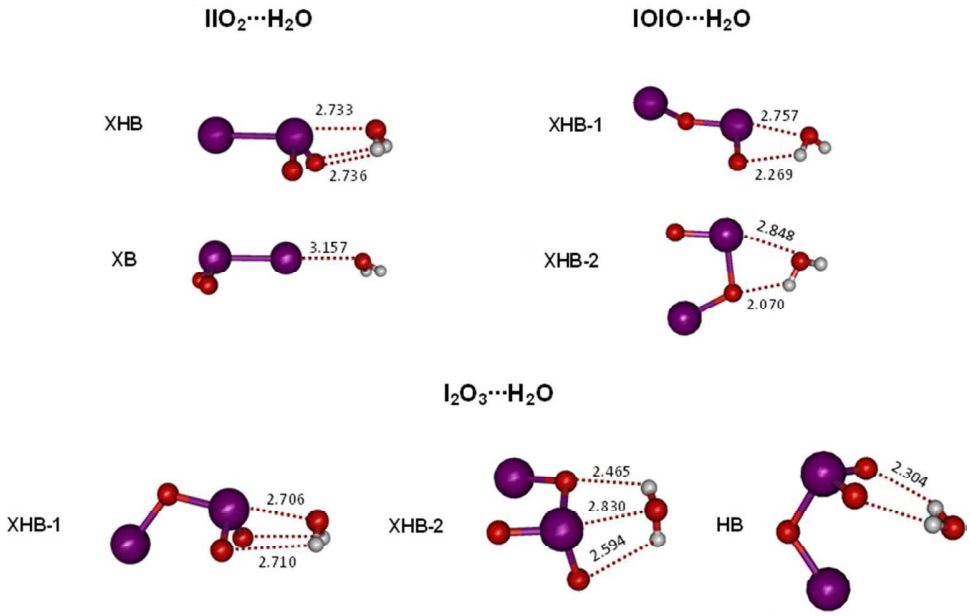

Figure 4. Caption: See manuscript
296x187mm (72 x 72 DPI)

View Article Online
DOI: 10.1039/C3CP51219C

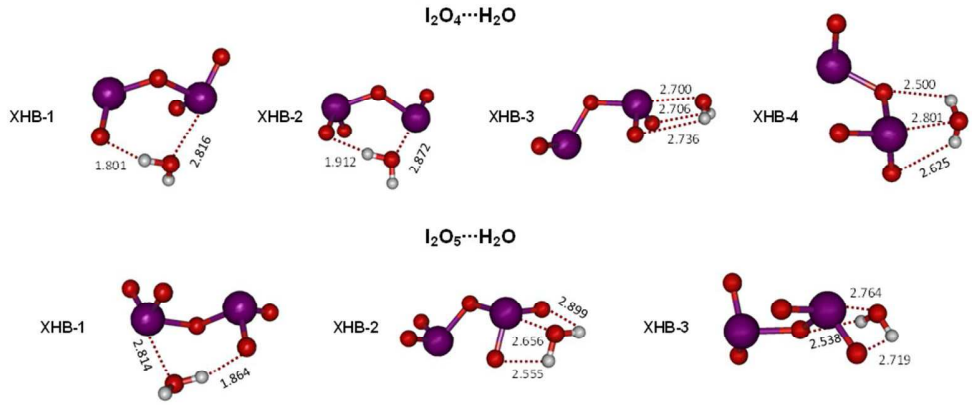

Figure 5. Caption: See manuscript
357x149mm (72 x 72 DPI)

View Article Online
DOI: 10.1039/C3CP51219C

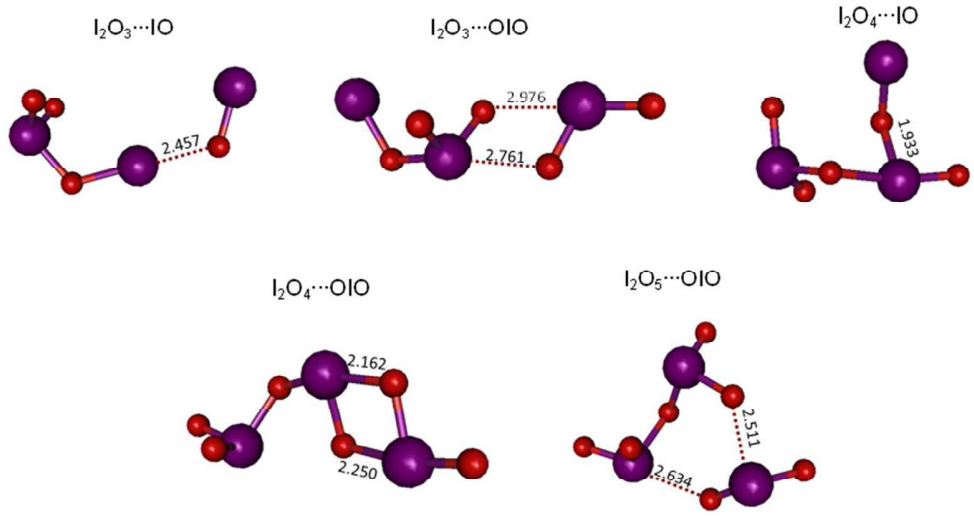

Figure 6. Caption: See manuscript
290x154mm (72 x 72 DPI)

View Article Online
DOI: 10.1039/C3CP51219C

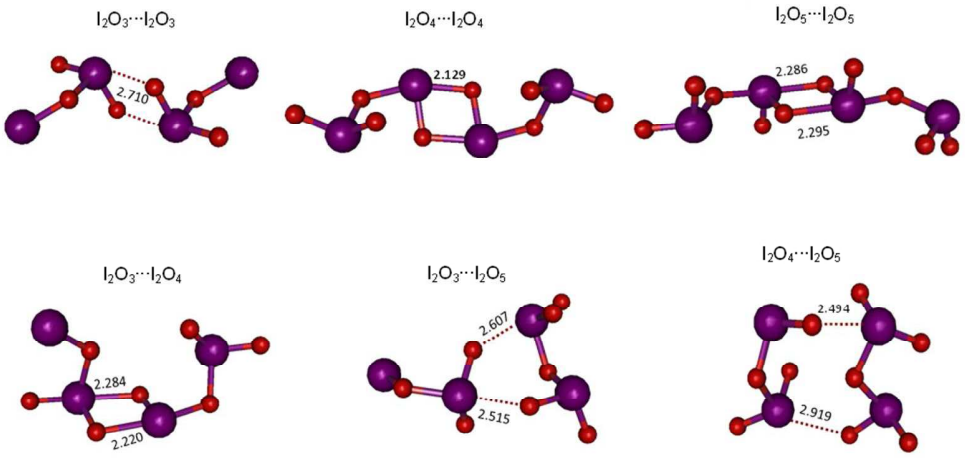

Figure 7. Caption: See manuscript
354x166mm (72 x 72 DPI)

View Article Online
DOI: 10.1039/C3CP51219C

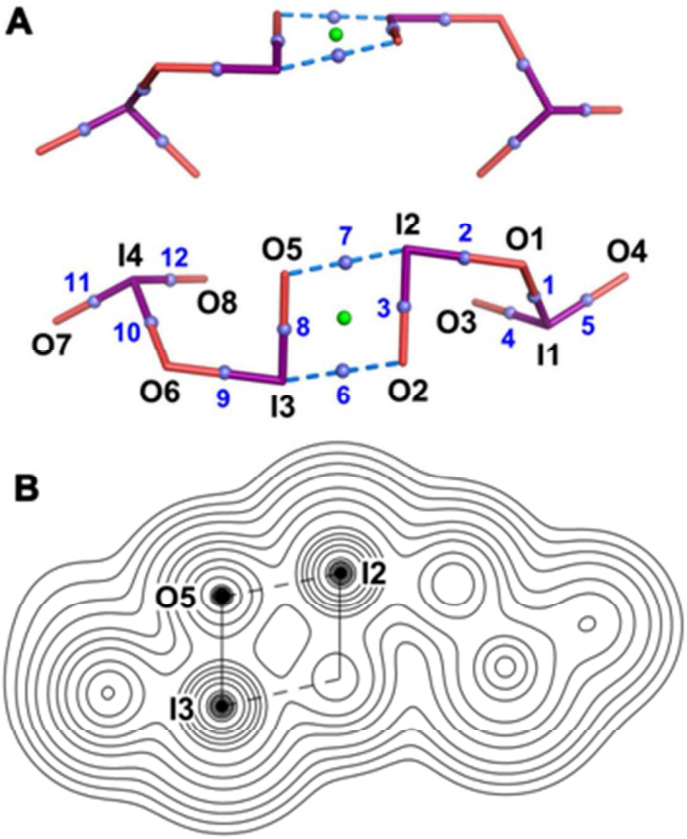

Figure 8. Caption: See manuscript
133x160mm (72 x 72 DPI)